

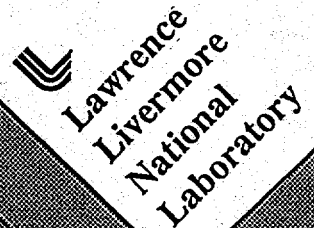
**Spectroscopic investigations of hard x-ray emission from 120 ps
laser-produced plasmas at intensities near 10^{17} W cm $^{-2}$**

J. Dunn, B.K.F. Young, A.L. Osterheld, M.E. Foord, R.S. Walling, and R.E. Stewart
Lawrence Livermore National Laboratory

Anatoly Ya. Faenov
VINIFTRI, Mendeleevo, Moscow Region, 141570, Russia

This paper was prepared for submittal to the
"Applications of Laser Plasma Radiation II," SPIE vol. 2523,
Organized by the International Society for Optical Engineering,
San Diego, California, July 12-14, 1995

November 1995



Lawrence
Livermore
National
Laboratory

This is a preprint of a paper intended for publication in a journal or proceedings. Since changes may be made before publication, this preprint is made available with the understanding that it will not be cited or reproduced without the permission of the author.

DISCLAIMER

This document was prepared as an account of work sponsored by an agency of the United States Government. Neither the United States Government nor the University of California nor any of their employees, makes any warranty, express or implied, or assumes any legal liability or responsibility for the accuracy, completeness, or usefulness of any information, apparatus, product, or process disclosed, or represents that its use would not infringe privately owned rights. Reference herein to any specific commercial products, process, or service by trade name, trademark, manufacturer, or otherwise, does not necessarily constitute or imply its endorsement, recommendation, or favoring by the United States Government or the University of California. The views and opinions of authors expressed herein do not necessarily state or reflect those of the United States Government thereof, and shall not be used for advertising or product endorsement purposes.

RETRAM

DISCLAIMER

**Portions of this document may be illegible
in electronic image products. Images are
produced from the best available original
document.**

Spectroscopic investigations of hard x-ray emission from 120 ps laser-produced plasmas at intensities near 10^{17} W cm $^{-2}$

J. Dunn, B. K. F Young, A. L. Osterheld, M. E. Foord, R. S. Walling, and R. E. Stewart

Lawrence Livermore National Laboratory, P.O. Box 808, Livermore, CA 94551 USA

Anatoly Ya. Faenov

VINIIFTRI, Mendeleevo, Moscow Region, 141570, Russia

ABSTRACT

Spectroscopic investigations of the x-ray emission of plasmas heated by 120 ps, frequency doubled pulses from the JANUS Nd:glass laser are presented. High Z K-shell spectra emitted from slab targets heated to near 10^{17} W cm $^{-2}$ intensity are investigated. High resolution ($\lambda/\Delta\lambda > 5000$) x-ray spectra of multicharged ions of He-like Ti, Co, Ni, Cu, and also H-like Sc in the spectral range 1.5 – 3.0 Å are obtained in single laser shots using a spherically bent Mica crystal spectrograph with a 186 mm radius of curvature. The spectra have one dimensional spatial resolution of about 25 μm and indicate that the size of the emission zone of the resonance transitions is < 25 μm. Simultaneous x-ray images of the plasma from a charge-coupled device pinhole camera confirmed that the plasma x-ray emission is from a similar sized source. Survey spectra ($\lambda/\Delta\lambda = 500-1000$) taken with a flat LiF (200) crystal spectrometer with a charge-coupled device detector complement the high resolution data. Two dimensional LASNEX modeling of the laser target conditions indicate that the high K-shell charge states are produced in the hot dense region of the plasma with electron temperature > 2 keV and density $\sim 10^{22}$ cm $^{-3}$. These experiments demonstrate that with modest laser energy, plasmas heated by high-intensity 120 ps lasers provide a very bright source of hard ~ 8 keV x-ray emission.

1. INTRODUCTION

In recent years, laser-produced plasmas have been investigated and characterized as a source of intense K-, L- and M-shell x-radiation¹⁻⁴. These experiments have involved the use of medium to large laboratory Nd:glass laser facilities with deliverable energies ranging from tens of joules^{1,3,4} to kilojoules². Pulse durations of ~ 100 ps¹⁻⁴ to in excess of 500 ps^{1,2} of fundamental, frequency doubled or tripled light have been used. Focusing conditions of 40 - 500 μm diameter spot sizes and 10^{14} - 10^{17} W cm $^{-2}$ intensities have been examined previously.

In this paper we present results from the Janus Nd:glass laser with 120 ps pulse of frequency doubled light. Solid interaction experiments at peak irradiances near 10^{17} W cm $^{-2}$ are achieved by tight focusing to a ~ 12 μm spot. We show that high temperature, dense, well-confined plasmas are generated which can ionize medium to high Z targets e.g. copper to the K-shell. We use a combination of high resolution and survey spectrometers with x-ray imaging capabilities to study single-shot spectra in the range 1.5 – 3.0 Å.

2. EXPERIMENTAL DESCRIPTION

A single 120 - 130 ps (FWHM) Gaussian shaped pulse of the JANUS Nd:glass laser was frequency doubled in a KDP crystal to 0.53 μm wavelength. A mean conversion efficiency of 47% from the fundamental was achieved for 1ω energies of 9 - 37 J as shown in Figure 1 (a). This gave a maximum of 17 J energy on target. Laser beam diagnostics monitored the pulse duration and energy for each shot. Figure 1 (b) shows the near Gaussian temporal pulse shape of the fundamental wavelength measured by an optical streak camera: the frequency doubled pulse shape and duration will be very similar.

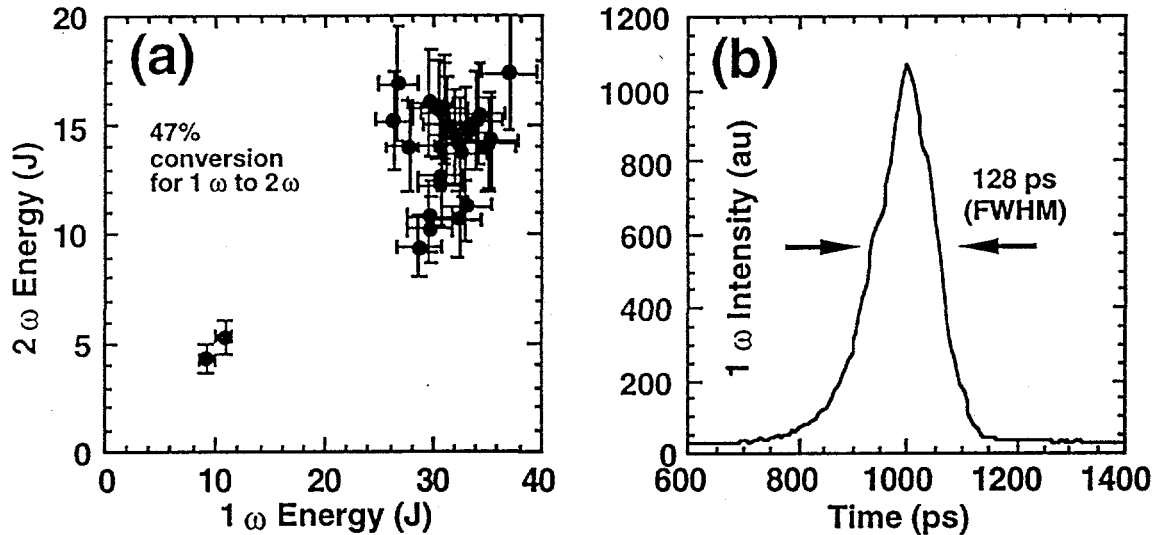


Figure 1(a) shows 2ω energy achieved as a function of 1ω energy after frequency doubling in a KDP crystal. Figure 1 (b) indicates the near Gaussian temporal shape of the 1ω pulse measured, before frequency doubling, with an optical streak camera.

The laser beam was relayed to the vacuum target chamber and focused with an aspheric $f/2$ lens of 20 cm focal length. The focal spot was imaged onto a calibrated Hitachi KP-140 CCD video camera using an identical aspheric $f/2$ lens and a spherical lens with 2 m focal length. A coaxial Ar ion laser beam was used to assist in focusing and aligning the frequency doubled beam onto the target. Using the alignment beam, a focal spot of 5 - 6 μm (FWHM) was measured. The best focus of the 2ω beam at full power was 10 - 12 μm (FWHM) as determined from the size of the x-ray images of the focal spot measured by the x-ray CCD pinhole camera. Figure 2 (a) shows a filtered pinhole image of 8 keV x-rays emitted from a nickel foil target irradiated with 16 J energy. Figure 2 (b) shows the corresponding profile plot of the image in Figure 2 (a). The x-ray images indicate that the spot is uniform, well focused and exhibits no structure or hot spots. The maximum peak irradiance of 2ω light on target, taking account of the approximately Gaussian focal spot and pulse shapes, was in the range of $0.9 - 1.2 \times 10^{17} \text{ W cm}^{-2}$. A repetition rate of one shot/30 min. was possible at full power.

The targets were constructed from flat 25 μm metal foils (Sc, Ti, Co, Ni and Cu) glued onto a 200 μm thick optically polished Si wafer. Accurate positioning of the laser onto the foil surface was achieved by first imaging the retro-reflection of the focused beam onto the polished Si wafer. This allowed us to place the foil surface to the desired laser focus position to within 25 μm along the laser axis. On all shots the target surface was perpendicular to the laser beam.

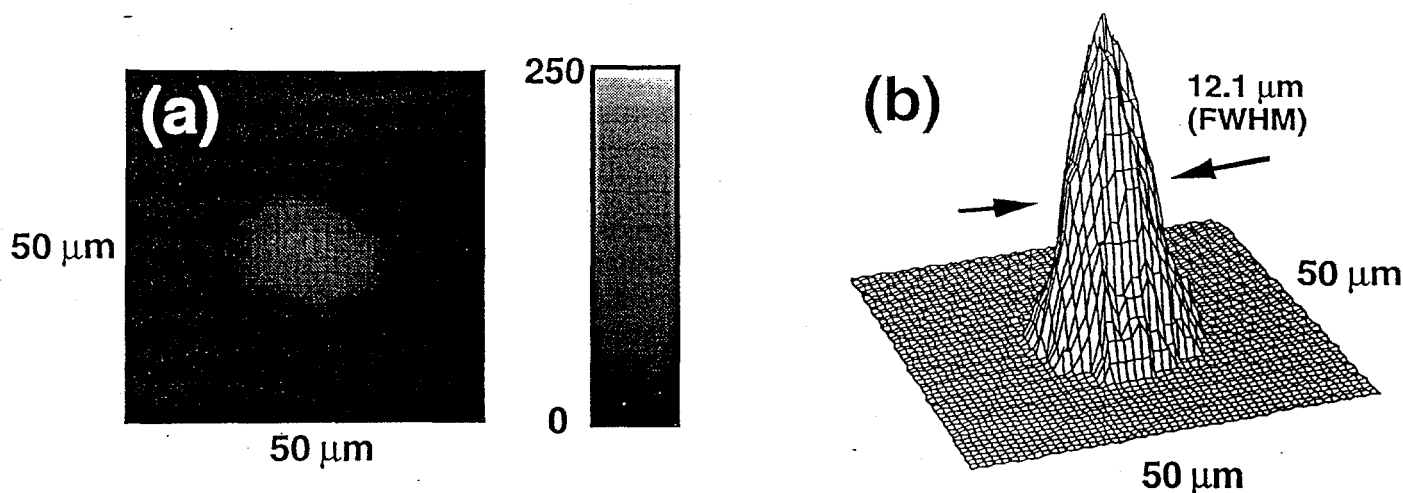


Figure 2 (a) is a filtered CCD pinhole image of 8 keV x-rays emitted from a nickel foil irradiated at $8 \times 10^{16} \text{ W cm}^{-2}$. Figure 2 (b) is a profile plot of (a).

A suite of x-ray diagnostics were used to spatially and spectroscopically resolve the plasma x-ray emission. A flat LiF (200), $2d=4.027 \text{ \AA}$, crystal mini-spectrometer recorded survey spectra to wavelengths of 1.5 \AA with medium resolving power, $\lambda/\Delta\lambda=500-1000$. The spectra were recorded onto an x-ray sensitive video format charge-coupled device (CCD) camera as shown in the photograph of Figure 3 (a). The video images were acquired and digitized by an 8-bit frame capture board utilizing a NUBUS slot of a Macintosh II computer. Two filters of $13 \mu\text{m}$ Be were placed immediately over the CCD and the tantalum slits defining the entrance window. Additional filters could be added in front of the detector to attenuate the x-ray signal. This instrument viewed the target at $\phi=0^\circ$, $\theta=45^\circ$, where θ is the polar angle measured from the laser axis and ϕ is the azimuthal angle.

Two versions of the high resolution Mica (002), $2d=19.84 \text{ \AA}$, Focusing spectrograph with Spherical dispersive element and Spatial Resolution (FSSR) were used⁵ with a crystal bent to a spherical radius of curvature of 100 mm and 186 mm, respectively. Figure 3 (b) shows a photograph of the $R=100\text{mm}$ version

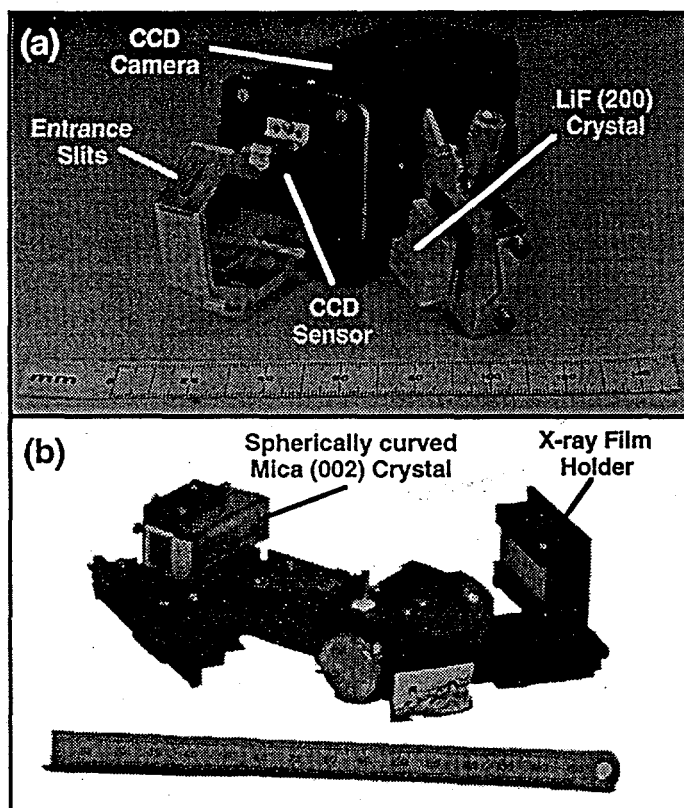


Figure 3 shows the compact spectrometers used in the experiment. (a) shows an exploded view of the flat crystal x-ray CCD survey spectrometer. The main features including the LiF (200) crystal, entrance slits, CCD camera and sensor are indicated. (b) shows the main features of the high resolution $R=100 \text{ mm}$ spherically curved Mica FSSR1 instrument.

of the FSSR. These instruments are distinguished by having efficient signal collection, high resolving power, $\lambda/\Delta\lambda > 5000$, and one dimensional spatial resolution of $< 30 \mu\text{m}$, perpendicular to the dispersion axis. The FSSR spectrographs observed the x-ray emission lines at high Bragg angles, $\theta_B > 70^\circ$, by using the high reflection efficiency of mica in multiple orders, up to $n=12$. The spectra were recorded on flat film packs of Kodak DEF x-ray film tangential to the Rowland circle and filtered with $13 \mu\text{m}$ Be. The FSSR1 was placed at $\phi=45^\circ$, $\theta=70^\circ$; the FSSR2 was positioned at $\phi=45^\circ$, $\theta=50^\circ$.

A $15\times$ magnification x-ray pinhole camera⁶ using a similar video format CCD detector monitored the plasma x-ray emission from the focal spot. An array of $5 \mu\text{m}$ pinholes with a total of $26 \mu\text{m}$ Be could resolve features to $\sim 5 \mu\text{m}$ spatial resolution. A filter wheel with Mylar filters up to $390 \mu\text{m}$ thick could be rotated remotely to adjust the x-ray intensity onto the CCD detector and reduce the sensitivity to soft x-ray emission below 2 keV for the high Z target x-ray conversion efficiency measurements. Source to pinhole distance was 15 mm. The pinhole camera was placed at $\phi=0^\circ$, $\theta=45^\circ$.

3. SPECTROSCOPIC RESULTS

Time-integrated K-shell spectra were recorded on the x-ray spectrometers for the following target materials: silicon, scandium, titanium, cobalt, nickel and copper. Strong He-like and H-like line emission were observed from silicon ($Z=14$) targets for intensities above $10^{14} \text{ W cm}^{-2}$. Spatially resolved spectra from the high resolution FSSR spectrometer indicated recombination emission occurring more than $50 \mu\text{m}$ in front of the target. A strong continuum was also observed. In contrast, the H-like series for scandium ($Z=21$) and titanium ($Z=22$) was very weak, just at the detection threshold, and not observed for cobalt ($Z=27$), nickel ($Z=28$) and copper ($Z=29$) targets. The titanium emission region was also noted to be spatially closer to the target surface. By studying the higher target atomic numbers, the K-shell x-ray emission was observed to be produced within $30 \mu\text{m}$ of the target.

We were able to observe strong He-like $1s^2 \ ^1S_0 - 1s2p \ ^1P_1$ resonance line and associated satellite spectra on single laser shots of 15 J energy as shown in the composite spectrum of Figure 4 for three different shots on cobalt, nickel and copper. This data was achieved with the flat crystal LiF (200) CCD survey spectrometer. The resonance and $1s^2 \ ^1S_0 - 1s2p \ ^3P_1$ intercombination lines are labeled, the latter being blended with unresolved $n = 2$ Li-like

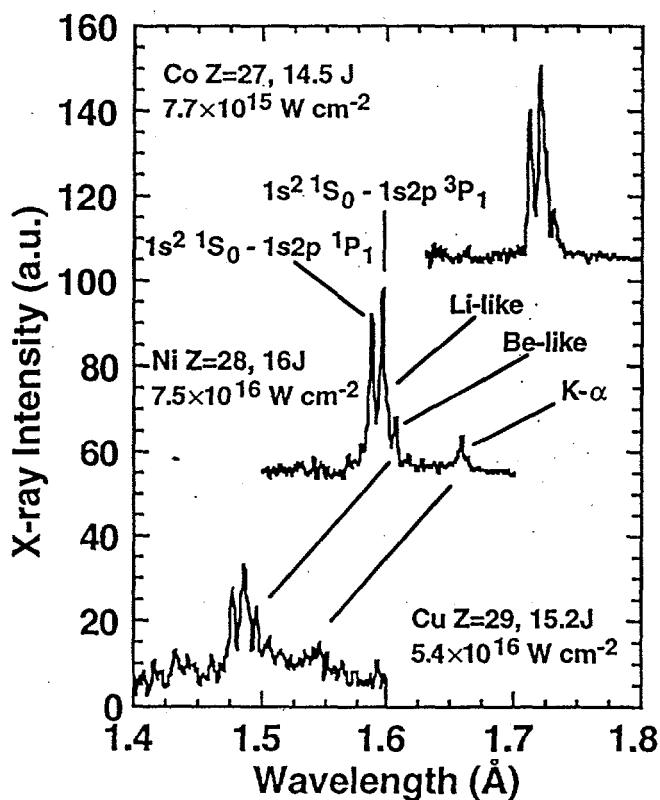


Figure 4 shows the heliumlike isoelectronic sequence for cobalt, nickel and copper, $Z= 27, 28, 29$ for 120 ps laser pulse widths and recorded with the CCD flat crystal survey x-ray spectrometer. All spectra are single shot: the energy and peak irradiance is noted. The Co K- α line at 1.79 \AA , top spectrum, was out of the spectral coverage.

lines. Additional Be-like lines features to the long wavelength side of the intercombination line are visible. The presence of the cold K- α fluorescence peak is indicative of suprathreshold electron production and has been previously noted in high Z K-shell spectra generated at high intensity^{1, 2}.

It is clear from this spectrum that Cu and possibly higher atomic numbers can be ionized to the He-like charge state. To our knowledge, this has not been observed previously for a 120 ps pulse width and opens up the possibility of studying very highly ionized matter at high density and temperature. To illustrate this further, Figure 5 (a) shows the He-like titanium spectrum recorded in 7th order on Kodak DEF film with the spherical R=186 mm Mica FSSR2 spectrometer: the increased instrumental resolving power reveals more details of the satellite spectra. The He-like and Li-like spectral features are labeled according to Gabriel⁷ and are identified using theoretical⁸ and experimental data⁹. The satellite lines are produced mainly by inner-shell excitation from the Li-like ground state or by dielectronic recombination from the He-like ion. A detailed discussion of this spectra is beyond the scope of the present paper. However, a comparison to the He-like titanium spectrum produced by 2ω , 1 ns pulse irradiation in Figure 5 (b) shows a number of differences relevant to the application of x-ray backlighters. Although the energy is $3\times$ higher for the spectrum of Figure 5 (b), no increased He-like resonance w line intensity is seen. Instead, the higher conversion efficiency reported later for 1 ns is due to the increased line intensity of the intercombination line y and satellite spectra. These lines are stronger mainly because of the lower plasma density, temperature and ionization conditions associated with the longer but lower intensity 1 ns pulse.

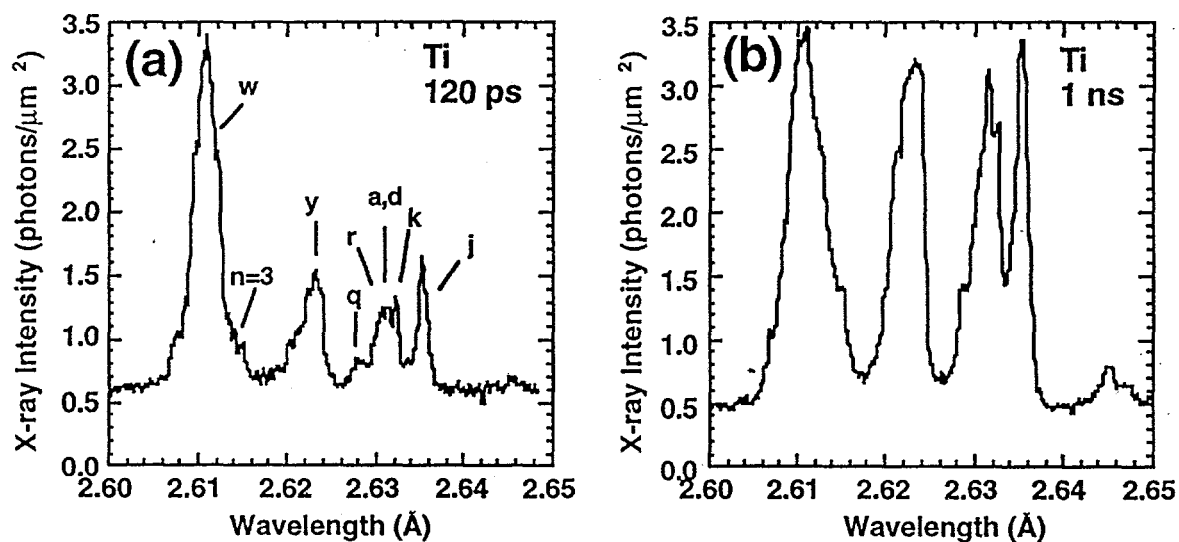


Figure 5 (a) shows a high resolution spectrum of He-like titanium produced by a 120 ps laser pulse at 10^{16} W cm⁻². The spectral features are labeled according to Gabriel⁷. Figure (b) is for the same target material but irradiated with $3\times$ more energy in a 1 ns laser pulse at lower 10^{15} W cm⁻² intensity.

4. HYDRODYNAMIC MODELING

The laser plasma conditions were simulated with the two-dimensional LASNEX hydrodynamic code¹⁰ using time-dependent non-LTE physics and an average atom ionization model. The code conditions were set as follows: 15 J energy of 0.53 μ m wavelength light in a 100 ps (FWHM) Gaussian pulse was focused to a 14 μ m (FWHM) near Gaussian spot at normal incidence to a titanium (Z=22) slab target. This produced a peak intensity of 4.5×10^{16} W cm⁻², within the intensity range of the experiment.

The plasma electron temperature is predicted to reach a maximum of 2.1 keV at the peak of the pulse at $t = 0$ ps; the surface layers are quickly ionized to the helium-like charge state at -100 to -50 ps, early in the laser pulse. However, overall only a few percent of hydrogenic titanium is produced, in agreement with the experimental observations. We plot the electron density n_e and emissivity profile at times -60 ps, 0 ps, and +60 ps to illustrate that the observed x-radiation is emitted from the high density conditions. Figure 6 (a) shows the electron density profile in front of the target. The initial target surface is at 0 μm . At $t = 0$ ps, the critical density surface, $n_c = 4 \times 10^{21} \text{ cm}^{-3}$, has evolved to $\sim 24 \mu\text{m}$ in front of the target. The peak electron temperature, however, is mainly in the overdense region from 10 to 27 μm . The result is that the most intense K-shell emission is expected to be weighted to high densities close to the target surface. This is confirmed in Figure 6 (b) which plots the x-ray emissivity profile, units of Watts cm^{-3} , integrated from 2.5 keV to 10 keV, for the same times in Figure 6 (a). Peak emissivity occurs at the peak of the pulse. At early time $t = -60$ ps, the titanium emission is higher than later in time as a result of the fast ionization to the He-like charge state. The emission region at $t = -60$ ps and 0 ps is $\sim 5 \mu\text{m}$ (FWHM) and 10 μm (FWHM), respectively. The position in z of peak emissivity at times $t = -60$ ps and 0 ps corresponds to electron density in excess of $n_e \sim 4 \times 10^{22} \text{ cm}^{-3}$, one order of magnitude higher than the critical density. The emissivity drops quickly on the trailing edge of the laser pulse indicating that the high Z K-shell emission follows the laser pulse shape as observed by Phillion and Hailey³. The simulations also indicate that the time-integrated K-shell emission is radiated within 20 μm from the target surface as observed by the high resolution imaging spectrometer and pinhole camera.

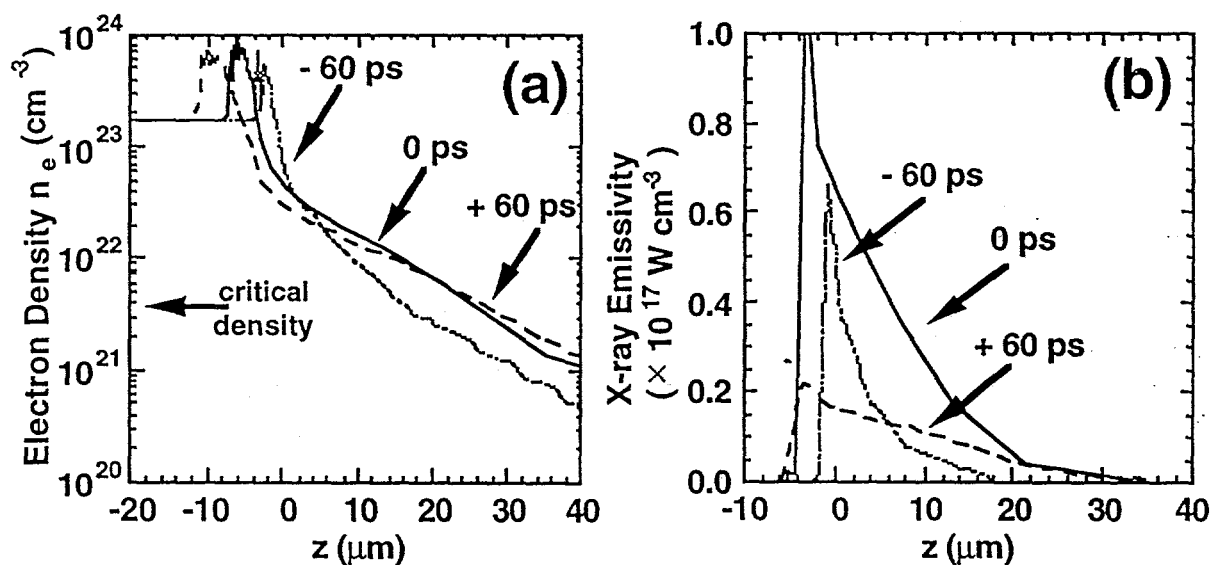


Figure 6(a) and (b) show 2-D LASNEX simulations of density and x-ray emissivity, respectively, as a function of distance z from the target for a titanium slab irradiated at $5 \times 10^{16} \text{ W cm}^{-2}$ at times $t = -60, 0, 60$ ps. Time $t = 0$ ps corresponds to the peak of the laser pulse. The x-ray emissivity is integrated over the 2.5 - 10 keV energy band.

5. X-RAY CONVERSION AND DISCUSSION

The CCD mini-spectrometer and CCD pinhole camera were used to measure the absolute conversion of the laser energy into K-shell x-rays. Using the known calibration of the crystal reflectivity, filter transmission and CCD x-ray response, the simple geometry of this instrument could be used to determine the absolute plasma x-ray emission. In practice, the x-ray emission and conversion efficiency were

determined using the x-ray CCD pinhole camera having taken account of the normalized spectrum recorded by the flat crystal CCD spectrometer.

The EEV CCD camera gain, linearity and full well capacity were determined from manufacturer's data¹¹ and optical calibration procedures. In order to deconvolve the recorded x-ray signal from the collected charge, the x-ray quantum detection efficiency (QDE) as a function of x-ray energy was calculated from a simple model using the absorption coefficient data from Veigele¹² and Henke *et al*¹³: no modeling of charge diffusion was included. The detailed CCD architecture for EEV P86000 standard video devices was used^{14, 15} assuming a 4 μm depletion layer in 20 μm thick epitaxial silicon¹⁶. Figure 7 (a) shows the predicted quantum detection efficiency for 0.5 - 10 keV x-rays. This is in good agreement with the standard device QDE curve from Figure 2 of Castelli *et al*¹⁴. The reduction in detection efficiency at low x-ray energies < 1.5 keV is a result of absorption within the passive surface oxide layers and polysilicon gate structure. At energies above 5 keV, the detection efficiency drops due to the increased absorption length for penetrating radiation in silicon. There may be an additional contribution to the detection efficiency from the field-free region immediately below the depletion region. We estimate that this may increase the quantum detection efficiency by as much as 50% at 8 keV and would have a consequence of lowering the high energy conversion measurements plotted in Figure 8.

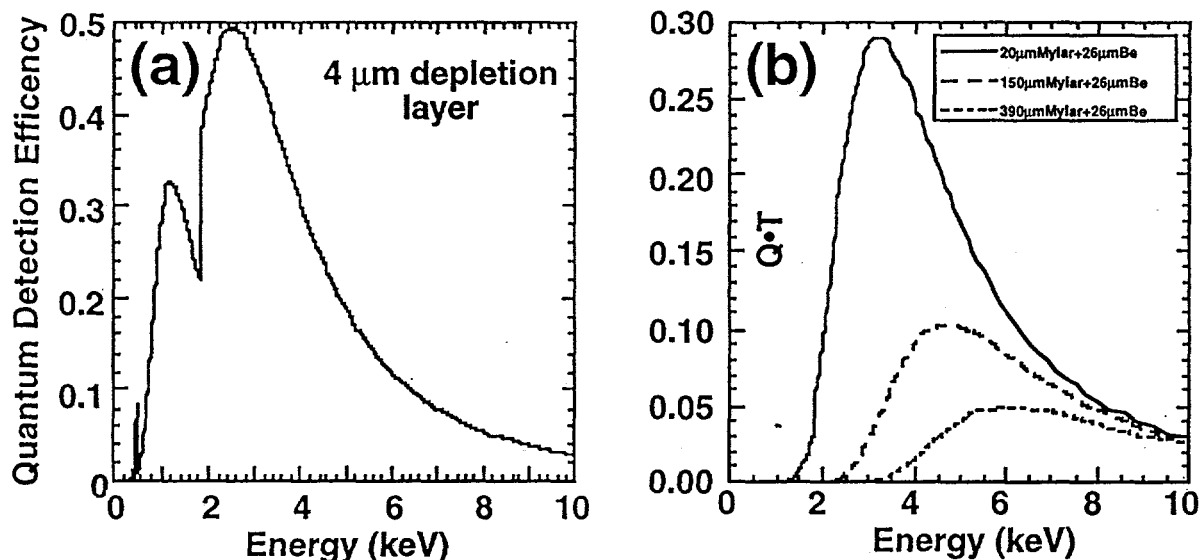


Figure 7(a) shows the CCD camera quantum detection efficiency as a function of incident x-ray energy using a 4 μm depletion layer active region. Figure 7(b) shows the quantum detection efficiency \times filter transmission product ($Q \cdot T$) for the filter sets used in the experiment. The thicker layers of 150 μm and 390 μm Mylar are used for the higher Z targets in order to reduce the sensitivity to L-shell emission below 2 keV.

Absorption filters of 150 μm and 390 μm Mylar were used to reduce the CCD detector sensitivity to low energy emission below ~ 2 keV from L-shell transitions for the high Z targets. An additional 26 μm Be layer was placed over the CCD sensor to filter all visible and UV light. Figure 7 (b) shows the detection efficiency \times filter transmission product as a function of x-ray energy for the different filter combinations used in the experiment. The 20 μm Mylar and 26 μm Be was used for the Si targets.

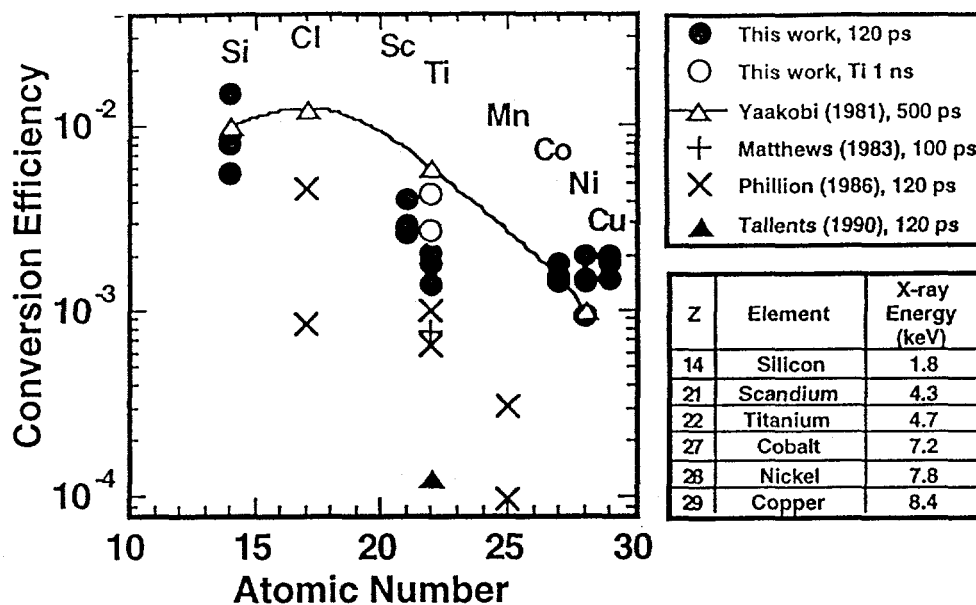


Figure 8 shows the conversion efficiency into K-shell x-rays for the atomic numbers $Z = 14$ to 29, silicon to copper, after Figure 2 of Yaakobi *et al*¹. Each data point (\bullet) of this work is an average of the conversion measured from three x-ray images taken for each 120 ps shot. 1 ns data points (\circ) are shown from this work. A line joining the data points of Yaakobi *et al*¹ taken with 500 ps, 3ω light at $5 \times 10^{14} \text{ W cm}^{-2}$ helps guide the eye. Other 120 ps data from Matthews *et al*², Phillion and Hailey³, and Tallents *et al*⁴ is included.

Figure 8 shows a plot of the K-shell x-ray conversion efficiency as a function of atomic number for silicon ($Z=14$) to copper ($Z=29$) after Figure 2 of Yaakobi *et al*¹. We define the x-ray conversion efficiency parameter to be the radiated K-shell x-ray energy expressed as a fraction of the incident laser energy. In addition to the $n = 2 - 1$ He-like lines with associated satellite spectra, we include the higher order He-like lines in the conversion calculation. This will have the effect of increasing the conversion slightly in comparison with other reported data: most authors include only the $n = 2 - 1$ He-like lines with associated satellite spectra and the $n = 2 - 1$ H-like line when observed. The data points for high Z atomic numbers ($Z = 21 - 29$) are measured for peak irradiances of $\sim 10^{16} - 8 \times 10^{16} \text{ W cm}^{-2}$; the lower intensity is achieved by keeping the laser energy constant and defocusing the focal spot. The conversion efficiency is $0.9 - 2.0 \times 10^{-3}$ for Ti, Co, Ni, and Cu while slightly higher for Sc at $2 - 4 \times 10^{-3}$. X-ray conversion of $0.8 - 1.5 \times 10^{-2}$, corresponding to $2.8 - 5.2 \times 10^{13}$ photons/ (Joule sphere) at 1.8 keV x-ray energy, is measured for silicon ($Z=14$) targets irradiated at a peak intensity of $4 \times 10^{15} \text{ W cm}^{-2}$. Strong hydrogenic and helium like emission are observed. In addition, a strong recombination continuum is observed for silicon but not for the higher Z targets as reported previously¹.

This work can be compared with similar results for slab targets irradiated by 120 ps 2ω light from Matthews *et al*², Phillion and Hailey³ and Tallents *et al*⁴ and 500 ps 3ω data from Yaakobi *et al*¹. These experiments, with the exception of Matthews *et al*², are at lower $10^{14} - 10^{16} \text{ W cm}^{-2}$ intensities. We neglect a comparison with data using 1ω light on the grounds that the lower plasma absorption produces lower x-ray conversion¹. However, higher K- α fluorescence has been observed from high Z targets using 1ω light at high intensity^{1, 2} where more laser energy is absorbed into suprathermal electrons.

There is significant variation in the reported conversion by different authors. For example, the titanium data varies from 1.3×10^{-4} for Tallents *et al*⁴ to 1×10^{-4} for Phillion and Hailey³. Some of this variation can be explained by intensity dependence as shown by Phillion and Hailey³. The data from Yaakobi *et al*¹, 40J of 3ω laser light in 500 ps pulse focused to 5×10^{14} W cm⁻² shows the highest x-ray conversion of the previously published data. They also report nearly the same conversion for 100 ps laser pulses for Si through Ni targets. The data in the present work is similar in a number of respects. We observe the same trend where silicon has the highest conversion $\sim 1\%$ falling to 0.1 - 0.2 % for nickel and copper. The higher x-ray conversion is observed to come from the defocused laser shots in agreement with previous observations^{1, 3}. In this work, the x-ray conversion as a function of atomic number falls more slowly. The nickel and copper conversion is slightly higher than previous work. We attribute this to the high energy-density plasma conditions near 10^{17} W cm⁻², as shown by the 2D LASNEX simulations of Figure 6.

Finally, we compare the x-ray conversion efficiency for 120 ps with 1 ns pulse duration for frequency doubled light focused on titanium slabs. Using a peak intensity of 1.3×10^{15} W cm⁻² for the 1 ns pulse we observe $\sim 2\times$ higher conversion, $2.8 - 4.4 \times 10^{-3}$, as plotted on Figure 8. This is closer to the 6×10^{-3} result measured for the 500 ps, 3ω pulse of Yaakobi *et al*¹. We would conclude that the 120 ps pulse is still preferable because the shorter duration of the x-ray emission produces a $5\times$ increase in line brightness.

6. SUMMARY

In conclusion, we have shown that a frequency doubled 120 ps laser pulse containing modest energy can be tightly focused to generate peak irradiances near 10^{17} W cm⁻². Solid targets of medium to high Z ($Z=14, 21-29$) materials irradiated under these conditions become highly ionized to the K-shell; specifically to the hydrogenic charge state for scandium and titanium ($Z=21, 22$) and to the heliumlike charge state for copper ($Z=29$). Time-integrated survey and high resolution spectra, recorded in the waveband 1.5 - 3.0 Å, are observed to be emitted from a small <20 μm, hot, dense plasma region and are consistent with hydrodynamic simulations. Plasma temperature and electron density are predicted to be $T_e \sim 2$ keV and $n_e > 10^{22}$ cm⁻³ at the peak of the laser pulse. These experiments demonstrate that a high Z laser-irradiated plasma can convert $\sim 1.5 \times 10^{-3}$ of the incident laser light into hard 8.4 keV K-shell x-rays giving yields of 10^{12} photons/ (Joule sphere).

7. ACKNOWLEDGMENTS

This experiment was conducted at the LLNL JANUS laser facility. The authors would like to thank Steve Shiromizu, Bill White, Allen Hankla and the JANUS laser staff for their excellent assistance in these experiments. Thanks also to Mark Eckart for continued support of this research. This work was performed under the auspices of the U.S. Dept. of Energy by the Lawrence Livermore National Laboratory under Contract No. W-7405-Eng-48.

8. REFERENCES

1. B. Yaakobi, P. Bourke, Y. Conturie, J. Delettrez, J. M. Forsyth, R. D. Frankel, L. M. Goldman, R. L. McRory, W. Seka, J. M. Soures, A. J. Burek and R. E. Deslattes, "High x-ray conversion efficiency with target irradiation by a frequency-tripled Nd:glass laser", *Opt. Commun.*, vol. 38(3), pp. 196, 1981.
2. D. L. Matthews, E. M. Campbell, N. M. Ceglio, G. Hermes, R. Kauffman, L. Koppel, R. Lee, K. Manes, V. Rupert, V. W. Slivinsky, R. Turner and F. Ze, "Characterization of laser-produced plasma x-ray sources for use in x-ray radiography", *J. Appl. Phys.*, vol. 54 (8), pp. 4260, 1983.
3. D. W. Phillion and C. J. Hailey, "Brightness and duration of x-ray line sources irradiated with intense 0.53- μm laser light at 60 and 120 ps pulse width", *Phys. Rev. A*, vol. 34(6), pp. 4886 (1986).
4. G. J. Tallents, M. H. Key, A. Ridgeley, W. Shaikh, C. L. S. Lewis, D. O'Neill, S. J. Davidson, N. J. Freeman, and D. Perkins, "An investigation of the x-ray point-source brightness for a short-pulse laser plasma", *J. Quant. Spectrosc. Radiat. Transfer*, vol. 43(1), pp. 53 (1990).
5. B. A. Bryunetkin, S. A. Pikuz, I. Yu. Skobelev, and A. Ya. Faenov, "Imaging spectroscopy of high temperature plasma sources", *Laser and Particle Beams*, vol. 10(4), pp. 849 (1992).
6. J. Dunn, B. K. Young and S. J. Shiromizu, "X-ray sensitive charge-coupled device instrumentation for short and ultra-short pulse laser-produced plasma experiments", *Rev. Sci. Instrum.*, vol. 66(1), pp. 706, (1995).
7. A. H. Gabriel, *Mon. Not. R. Astron. Soc.*, vol. 160, pp. 99 (1972).
8. L. A. Vainshtein and U. I. Safronova, "Satellites to resonance lines of H- and He-like ions, *Atomic Data and Nuclear Data Tables*, vol. 21(1), pp. 49 (1978).
9. M. Bitter, H. Hsuan, S. von Goeler, K.W. Hill, B. Grek, D. W. Johnson, and V. Decaux, "Measurements of dielectronic recombination rate coefficients for He-like and H-like metal ions from Tokamak plasmas", *Physica Scripta*, vol. T37, 66 (1991).
10. G. B. Zimmerman and W. L. Kruer, "Numerical simulation of laser-initiated fusion", *Comments Plasma Phys. Controlled Fusion*, vol. 2, pp. 51 (1975).
11. EEV Ltd., Waterhouse Lane, Chelmsford, Essex, CM1 2QU, England.
12. W. J. Veigele, "Photon cross sections from 0.1 keV to 1 MeV for elements $Z = 1$ to $Z = 94$ ", *Atomic Data*, vol. 5(1), pp. 51 (1973).
13. B. L. Henke, P. Lee, T. J. Tanaka, R. L. Tanaka, R. L. Shimabukuro and B. K. Fujikawa, "Low-energy x-ray interaction coefficients: photoabsorption, scattering, and reflection.", *Atomic Data and Nuclear Data Tables*, vol. 27(1), pp. 1 (1982).
14. C. Castelli, A. Wells, K. McCarthy and A. Holland, "Soft x-ray response of charge coupled devices", *Nucl. Instrum. and Meth.*, vol. A310, pp. 240 (1991).
15. P. Bailey and P. Pool, "The P88000 series of large area CCDs for visible, near infra-red, and x-ray scientific imaging applications", *Proc. SPIE* vol. 1344, pp. 356 (1990).
16. The EEV P45510 video camera used here has similar architecture to the P86000 standard video device. Private communication, H. F. Garvey, EEV Ltd., Waterhouse Lane, Chelmsford, Essex, CM1 2QU, England (1994).